# Experimental Characterization of V2I Radio Channel in a Suburban Environment

M. Yusuf[1], E. Tanghe[1], F. Challita[2], P. Laly[2], D. P. Gaillot[2], M. Liénard[2],
B. Lannoo[3], R. Berkvens[3], M. Weyn[3], L. Martens[1], and W. Joseph[1]
[1]IMEC-WAVES, Ghent University, Ghent, Belgium
[2]IEMN-TELICE, University of Lille, Lille, France
[3]IMEC-IDLab, University of Antwerp, Antwerp, Belgium

***Abstract*—This paper describes the results of the experimental vehicle-to-infrastructure radio channel sounding campaign at 1.35 GHz performed in a suburban environment in Lille, France. Based on the channel measurements acquired in vertical and horizontal polarizations, a multitaper estimator is used to estimate the local scattering function for sequential regions in time, from which Doppler and delay power profiles are deduced. We analyze second order statistics such as delay and Doppler spreads, as well as small-scale fading amplitude. A similar behavior between both polarizations is observed. In both cases, the statistical distributions of the RMS delay and Doppler spreads are best fitted to a lognormal model. The small-scale fading of the strongest path is found to be Rician distributed, while the later delay taps show occasional worse-than-Rayleigh behavior.**

***Index Terms*— vehicular, propagation, measurement, small-scale fading, delay spread, doppler spread, polarization**

## I. Introduction

Vehicular communications have recently attracted much interest due to the rapid development of wireless communication technologies. Through the integration of information and communication technologies, all road users can gather sensor data and share information about traffic and road-state dynamics with each other and with the road infrastructure. This envisioned intelligent transportation system (ITS) will improve the safety and efficiency of the transportation by enabling a wide range of applications [1]. Such systems require reliable low-latency vehicular-to-vehicular (V2V) and vehicular-to-infrastructure (V2I) communication links that provide robust connectivity at a fair data rate. An essential requirement for the development of such vehicular systems is the accurate modeling of the propagation channel in different scenarios and environments.

Some V2I propagation channels resemble existing cellular links, where one node is stationary, while the other node is mobile. However, the placement height and surroundings of the infrastructure nodes for vehicular communication are unique, resulting in different dominant propagation mechanisms [2]. One of the main challenges for vehicular communications that strongly differ from cellular networks is the rapidly time-varying radio propagation channel. As a result, the widely used assumption of wide-sense stationarity (WSS) uncorrelated scattering (US) channel is no longer satisfied [3], [4].

The non-stationary fading process of vehicular channels can be characterized by assuming local stationarity for a finite region in time and frequency. The author in [4] provides a theoretical framework that extends the scattering function of the WSSUS to a time-frequency (TF) dependent local scattering function (LSF). Based on the LSF, power profiles of delay (PDP) and Doppler (DPP) can be estimated, and subsequent analysis of the corresponding second central moments can be performed. The RMS delay and Doppler spreads are evaluated in [5] for several V2V scenarios, where a bimodal Gaussian mixture is used to model their statistical distribution. Other papers show the distribution of the spreads to follow a lognormal model [6], [7], [8]. However, these studies focus on the ITS licensed band around 5.9 GHz in other scenarios, and do not take channel polarization into consideration.

In this paper, we characterize the delay and Doppler of a channel sounding campaign in the LTE-V radio interface band that supports V2I communications (named Uu-interface) [9]. The environment is considered suburban with mainly LOS scenario. The RMS delay and Doppler spreads are evaluated and statistically modeled for horizontal and vertical polarizations. We also model the small-scale fading of the wideband channel taps. The outline of the paper is as follows. The description of measurements and methodology of analysis are presented in Section II. Section III describes the results and discussions, while conclusions are drawn in Section IV.

## II. Description of Measurements and Methodology

### A. Measurement setup and scenario

Channel measurements are performed with the MIMOSA radio channel sounder [10]. We use 80 MHz of transmission bandwidth centered around a carrier frequency of 1.35 GHz. The sounder uses dual-polarized patch antenna arrays with horizontal (H) and vertical (V) polarizations. For this measurement campaign, horizontal uniform linear arrays with 15 cm inter-element spacing (0.7 times the wavelength) are used at both the transmitter (Tx) and receiver (Rx). Fig. 1 shows the measurement setup. For Rx, we use one patch antenna in each traveling direction of the lanes, while Tx transmits using four patch antennas, two facing each direction. The channel sounder is fully parallel: the data from each transmit antenna is simultaneously modulated onto the carriers using interleaved frequency division multiple access. Table I summarizes the

Fig. 1. Tx as a roadside unit (left) and Rx patch antennas on top of the van (right)

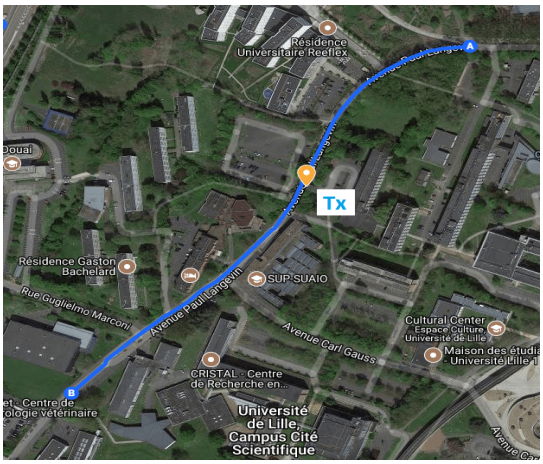


Fig. 2. Top view of measurement route at the university of Lille campus. Tx location is marked with a yellow pin and Rx van moves from point A to B. (Map data ©2018 Google)

TABLE I
MIMOSA CHANNEL SOUNDER SPECIFICATIONS

| Parameter | Setting |
|---|---|
| center frequency | 1.35 GHz |
| bandwidth | 80 MHz |
| antenna type | 120° HPBW patch antenna |
| number of Tx antennas | 4 |
| number of Rx antennas | 2 |
| Tx and Rx polarization | H/V |
| OFDM subcarriers per channel | 819 |
| OFDM symbol duration $T_S$ | 81.92 $\mu$s |
| cyclic prefix duration $T_{CP}$ | $0 \leq T_{CP} \leq T_S$ |
| full channel acquisition time | $2\,(T_S + T_{CP}) \leq 327.68$ $\mu$s |
| frame duration | 0.5 s |

technical specifications of the MIMOSA channel sounder used for this measurement campaign.

Measurements have been carried out at the campus of the university of Lille in France. The environment can be categorized as suburban: the road is narrow with one lane in each direction and buildings and vegetation are set back 5-8 m from the curb. In order to follow the V2I scenario, Tx is placed on the curb with the antenna placed at 2.5 m height. The Rx antenna is mounted on the rooftop of the van carrying Rx inside, as shown in Fig. 1. The van moves along the road at 30 kmp h speed, crossing the Tx position during a total route of 500 m, shown in Fig. 2. Due to some storage limitations of the channel sounder, we drop some samples during reception, which gives us a snapshot repetition time $t_s$ = 3.92 ms per frame. With these parameter settings, we achieve a maximum Doppler shift of $1/2t_s$ = 128 Hz and a minimum resolvable delay resolution of 12.5 ns.

### B. Methodology of analysis

Due to the high mobility of Tx, Rx and scatterers in vehicular communications, the environment is rapidly changing, and the observed fading process is non-stationary. The channel sounder provides a sampled measurement of the continuous channel transfer function (CTF) $H(t, f)$ that is time-varying and frequency selective. We collect $Q$ = 819 frequency bins over $B$ = 80 MHz measured bandwidth for each snapshot. The number of snapshots $S$ = 128 per frame, with a repetition time of $t_s$ = 3.92 ms. The discrete CTF is

$$H[m, q] = H(t_s m, f_s q) \tag{1}$$

where the frequency resolution $f_s = B/Q$, the time index $m \in \{0, ..., S-1\}$ and the frequency index $q \in \{0, ..., Q-1\}$

*1) LSF Estimate:* We use the discrete version of the LSF multitaper-based estimator proposed in [4]. The applied orthonormal 2-D tapering windows are computed from $K$ and $L$ orthogonal tapers in the time and frequency domains, respectively. We estimate the LSF for consecutive regions in time, within which the channel is assumed WSSUS. A sliding window is used with an extent of $M \times N$ samples in time and frequency, respectively. The time index of each region $k_t \in \{0, ..., \frac{S-M}{\Delta_t} - 1\}$ corresponds to its center, while $\Delta_t$ denotes the sliding time shift between consecutive estimation regions. The LSF estimate is formulated as

$$\hat{C}[k_t, n, p] = \frac{1}{LK} \sum_{w=0}^{LK-1} \left| H^{(G_w)}[k_t, n, p] \right|^2 \tag{2}$$

where $n \in \{0, ..., N-1\}$ denotes the delay index and $p \in \{-M/2, ..., M/2-1\}$ denotes the Doppler index. The windowed tapering function $H^{(G_w)}$ is calculated as

$$H^{(G_w)}[k_t, n, p] = \sum_{q'=-N/2}^{N/2-1} \sum_{m'=-M/2}^{M/2-1} G_w[m', q'] \; H[m' + \Delta_t k_t + M/2,\; q' + N/2] \; e^{-j2\pi(pm' - nq')} \tag{3}$$

where the relative time and frequency indexes within each region are $m'$ and $q'$, respectively, and the window functions $G_w$ are localized within the $[-M/2, M/2-1] \times [-N/2, N/2-1]$ region. The tapers are chosen as the discrete prolate spheroidal

sequences (DPSS) and the number of used tapers is $K = 2$ and $L = 2$ in both time and frequency domains. We choose the dimension in time domain $M = 64$ samples and we include the whole bandwidth of $N = Q = 819$ samples in frequency domain. The sliding time shift is selected to be half of the frame size, i.e. $\Delta_t = 64$ samples. With these parameters, we obtain a LSF estimate of delay resolution $\tau_s = 1/B = 12.5$ ns, and Doppler resolution $\upsilon_s = 1/(Mt_s) = 4$ Hz.

*2) Delay and Doppler Spreads:* The LSF is estimated for each Tx-Rx antenna pair, hence, a total of $4 \times 2 = 8$ links are evaluated. We consider the combined LSF to resemble a bidirectional antenna radiation pattern by averaging the LSF estimates of all 8 links. The PDP $\hat{P}$ and DPP $\hat{Q}$ are the projections of the combined LSF on the delay and Doppler domains, respectively. Based on (2), the time-varying profiles can be defined as

$$\hat{P}[k_t, n] = \frac{1}{M} \sum_{p=-M/2}^{M/2-1} \hat{C}[k_t, n, p]$$
$$\hat{Q}[k_t, p] = \frac{1}{N} \sum_{n=0}^{N-1} \hat{C}[k_t, n, p] \quad (4)$$

and the time-varying RMS delay and Doppler spreads can be calculated, respectively, as

$$\hat{\sigma}_\tau[k_t] = \sqrt{\frac{\sum_{n=0}^{N-1} (n\tau_s)^2 \hat{P}[k_t, n]}{\sum_{n=0}^{N-1} \hat{P}[k_t, n]} - \left( \frac{\sum_{n=0}^{N-1} n\tau_s \hat{P}[k_t, n]}{\sum_{n=0}^{N-1} \hat{P}[k_t, n]} \right)^2} \quad (5)$$

and

$$\hat{\sigma}_\upsilon[k_t] = \sqrt{\frac{\sum_{p=-M/2}^{M/2-1} (p\upsilon_s)^2 \hat{Q}[k_t, p]}{\sum_{p=-M/2}^{M/2-1} \hat{Q}[k_t, p]} - \left( \frac{\sum_{p=-M/2}^{M/2-1} p\upsilon_s \hat{Q}[k_t, p]}{\sum_{p=-M/2}^{M/2-1} \hat{Q}[k_t, p]} \right)^2} \quad (6)$$

Before calculating the spreads, pre-processing is carried out for each LSF separately. No significant multipath components are found with delay larger than 2 $\mu$s, so we limit the LSF to this value in the delay domain, and align all LSFs to the same absolute mean delay. In order to avoid spurious and noise components, we set all the components of the estimated LSF to zero that are: below the noise level plus 5 dB, and below the maximum value of a given LSF minus 40 dB.

*3) Small-scale fading:* The investigation of the small-scale amplitude is conducted in the delay domain across consecutive time frames. For that purpose, we apply an inverse discrete Fourier transform to the CTF in (1) using a Hanning window to obtain the time-varying channel impulse response (CIR). Then, we align the CIRs so that the maximum LOS components have the same absolute delay. Finally, we can estimate the small-scale fading by removing the path loss and large-scale fading using a moving average filter of the same size as the LSF estimation window.

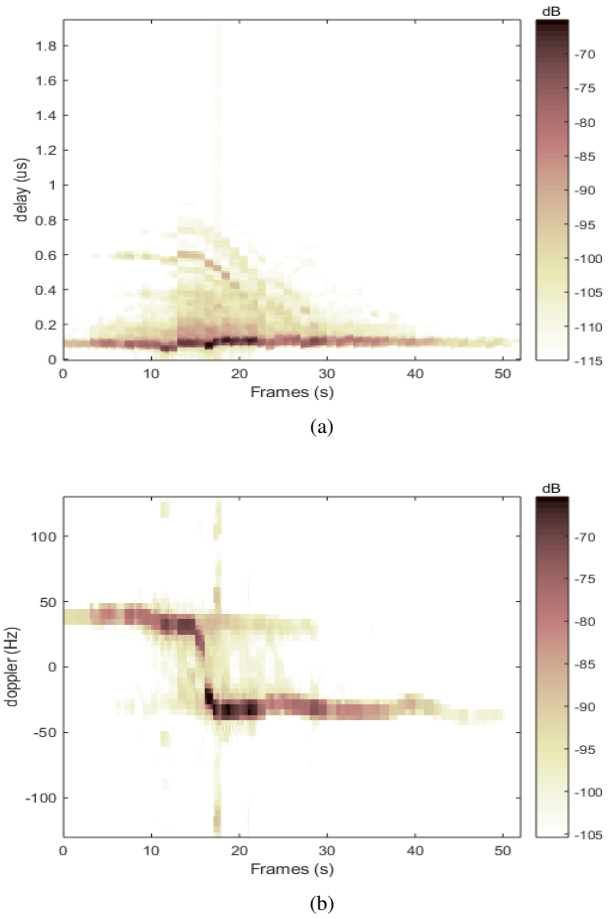


Fig. 3. Time-varying PDP (a) and DPP (b) of the V-polar channel for the crossing scenario with constant speed of 30 km/h

## III. Results and Discussion

### A. RMS Delay and Doppler Spreads

The PDP and DPP are depicted in Fig. 3 for the V-polar channel measurement, while the corresponding RMS delay and Doppler spreads are in Fig. 4. The two parameters are showing quite similar behaviors, specially after Rx crosses Tx position around 17 s, indicating a high correlation between both spreads. The Pearson product-moment correlation coefficient is calculated as 0.49 over all frames. Spread values are much smaller than typical values in cellular scenarios [11], [12] due to the domination of the LOS scenario.

In order to statistically characterize the spreads, we use the Kolmogorov-Smirnov (KS) test to select the distribution by comparing the p-value of different models: lognormal, normal, Nakagami, Rayleigh, Weibull, and Rician. It is found that the lognormal distribution gives the best fit to the measured parameters. Fig. 5 shows the histograms of the RMS delay

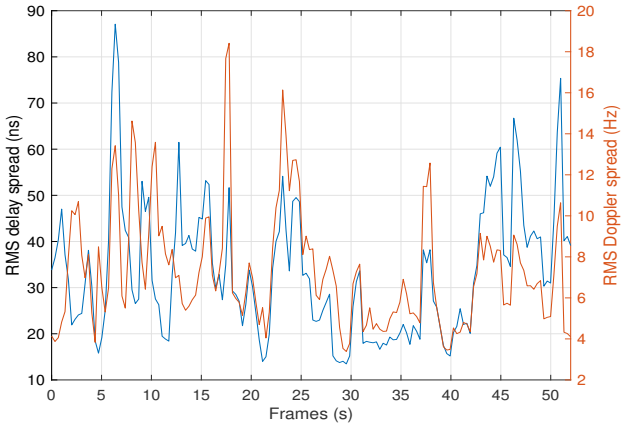


Fig. 4. RMS delay and Doppler spreads of the V-polar channel

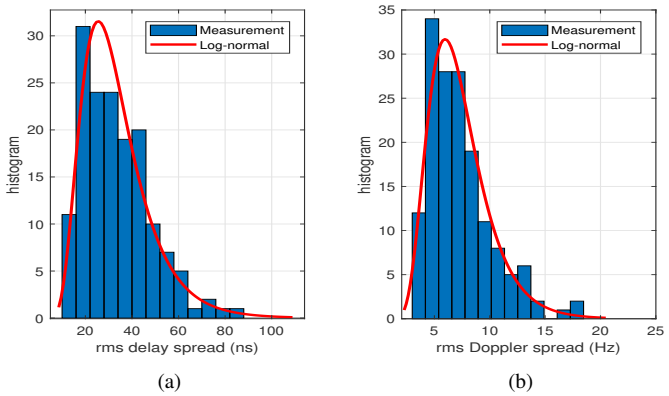


Fig. 5. Histograms of the (a) RMS delay spread and (b) RMS Doppler spread of the V-polar channel and the corresponding lognormal models

TABLE II
STATISTICS OF THE RMS DELAY AND DOPPLER SPREADS LOG-NORMAL DISTRIBUTION

| | | Mean | KS-test p-value | $\mu$ | $\sigma$ |
|---|---|---|---|---|---|
| $\hat{\sigma}_\tau$ | V | 33.39 ns | 0.52 | 3.42 | 0.42 |
| | H | 42.50 ns | 0.36 | 3.66 | 0.42 |
| $\hat{\sigma}_\upsilon$ | V | 7.31 Hz | 0.80 | 1.92 | 0.37 |
| | H | 10.26 Hz | 0.82 | 2.25 | 0.38 |

TABLE III
MEAN SIGNIFICANCE VALUE (P) AND SUCCESS RATE (%) OF THE KS-TEST FOR SMALL-SCALE FADING AMPLITUDE OF H-POLAR CHANNEL

| Tap | Rician | | Rayleigh | | Nakagami | | Weibull | |
|---|---|---|---|---|---|---|---|---|
| | (p) | (%) | (p) | (%) | (p) | (%) | (p) | (%) |
| 0 | 0.44 | 77.88 | 0.58 | 2.88 | 0.44 | 75.00 | 0.40 | 71.15 |
| 1 | 0.44 | 65.38 | 0.31 | 19.23 | 0.36 | 63.46 | 0.43 | 65.38 |
| 2 | 0.65 | 72.12 | 0.40 | 34.62 | 0.58 | 75.00 | 0.62 | 76.92 |
| 3 | 0.58 | 81.73 | 0.34 | 48.08 | 0.49 | 88.46 | 0.54 | 93.27 |

and Doppler spreads of the V-polar channel and their corresponding best fit models. Similar characteristics are found for the H-polar channel. Table II lists the details of the lognormal distributions for both channels, where it shows that the H-polar channel has slightly larger mean delay and Doppler spreads compared to the V-polar channel.

### *B. Small-scale Fading Amplitude*

Traditionally, the Rayleigh fading is the common assumption in mobile communications for worst-case performance analysis, while the Rician fading is used when there exists a dominant path component (e.g. LOS). However, more severe fading distributions have been reported, specially for vehicular communications where WSSUS assumptions are no longer valid [13], [14]. In this section, we aim to characterize the distribution of the small-scale fading amplitude per delay tap. According to Table II, the mean delay spread of both polarizations are well covered by the first 4 delay taps (50 ns). We again use the KS-test with a 95% confidence interval

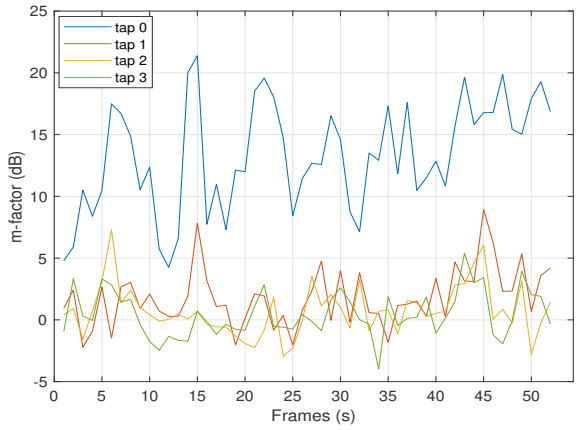


Fig. 6. m-factor estimate of the small-scale fading for the H-polar channel

per frame to compare the most common distributions: Rician, Rayleigh, Nakagami-m, and Weibull.

Table III lists the mean p-values of the H-polar channel frames that passed the KS-test and the success rate of each candidate distribution for the H-polar channel. Although all the p-values are satisfactory, deciding based on the p-values alone can be misleading. For example, while the Rayleigh model has the highest p-value for the first tap, it has the lowest success rate among the candidate models. Similar fading behavior is observed for the V-polar channel.

To better understand the behavior of each delay tap, we use a flexible parametric model to express the severity of fading. We estimate the Nakagami $m$-factor for the first 4 taps using the maximum-likelihood estimator [15]. The $m$ is also called the shape factor, since a larger $m$ means a decreasing fading depth. The $m$ estimate per frame for the 4 taps of the H-polar channel is depicted in Fig. 6. Indeed, the first tap has large values of $m > 1$ indicating a better-than-Rayleigh fading, while the other taps suffer from more severe fading with $m = 1$ (Rayleigh) and $m < 1$ (worse-than-Rayleigh).

Based on the previous analysis, we choose to model the

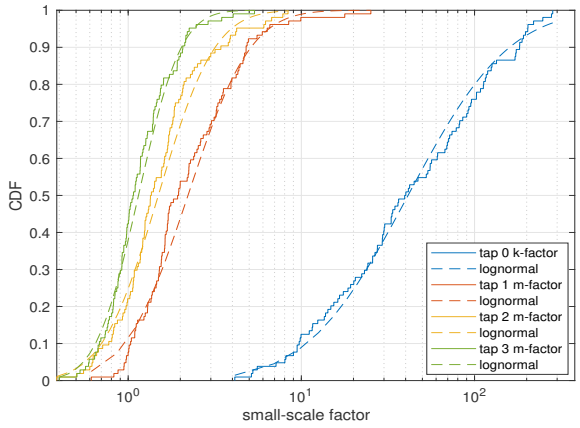


Fig. 7. Cumulative distribution function (CDF) of the small-scale fading parameters (K-factor for tap 0 and m-factor for later taps) and the corresponding lognormal models for the H-polar channel

TABLE IV
STATISTICS OF THE SMALL-SCALE FADING PARAMETERS LOG-NORMAL DISTRIBUTION

| Tap | | Mean (dB) | KS-test p-value | $\mu$ | $\sigma$ |
|---|---|---|---|---|---|
| 0 | V | 19.68 | 0.22 | 4.11 | 1.02 |
| (K-factor) | H | 18.30 | 0.77 | 3.72 | 1.05 |
| 1 | V | 4.13 | 0.13 | 0.66 | 0.66 |
| (m-factor) | H | 4.61 | 0.11 | 0.80 | 0.65 |
| 2 | V | 1.85 | 0.37 | 0.20 | 0.61 |
| (m-factor) | H | 2.60 | 0.23 | 0.40 | 0.59 |
| 3 | V | 2.80 | 0.15 | 0.41 | 0.64 |
| (m-factor) | H | 1.07 | 0.48 | 0.14 | 0.45 |

first tap with a Rician fading as it has the highest success rate. However, for the later taps, we select the Nakagami-m fading. While both the Weibull and Nakagami models have higher success rates, the Nakagami distribution is widely studied in the literature and can be treated more easily in theoretical investigations, compared to the purely empirical Weibull distribution [6]. The K-factor of the first tap is estimated using the method of moments [16]. Fig. 7 shows the best fit lognormal model to the statistical distribution of the estimated parameters for the H-polar channel, and Table IV lists the statistics of the lognormal models for H and V channels. We notice that the mean K-factor of the first tap (tap 0) is slightly larger for the V-polar channel than for the H-polar channel. This is consistent with the results in Table II that show larger mean delay and Doppler spreads for the H-polar channel. A reason for that can be stronger scattering components in H-polar from ground and other reflectors with larger horizontal geometry (e.g. vehicles).

## IV. Conclusion

Based on a measurement campaign in Lille, France, we characterize the V2I channel in a suburban environment for vertical and horizontal polarizations. For this non-stationary fading channel, the LSF is estimated and used to calculate the time-varying delay and Doppler power profiles. The corresponding second central moments are evaluated and modeled statistically. It is found that a lognormal model best fits the RMS delay and doppler spreads. Both polarizations show a similar behavior, with the mean spreads of H-polar channel being slightly larger than V-polar channel. The small-scale fading is investigated per delay tap. The parameters of the Rician fading for the first tap and Nakagami fading for the later taps are estimated and statistically modeled. The best fit is found to be the lognormal model.

## Acknowledgment

This research was supported by the VLAIO project "Smart Highway" and the EOS project "Multi-service Wireless Network (MUSE-WINET)".

## References

[1] Intelligent Transport Systems (ITS); Vehicular Communications; Basic Set of Applications; Definitions, ETSI TR 102 638 V1.1.1, Tech. Rep., 2009.

[2] C. F. Mecklenbrauker, A. F. Molisch, J. Karedal, F. Tufvesson, A. Paier, L. Bernadó, T. Zemen, O. Klemp, and N. Czink, "Vehicular channel characterization and its implications for wireless system design and performance," *Proceedings of the IEEE*, vol. 99, no. 7, pp. 1189–1212, 2011.

[3] L. Bernadó, T. Zemen, F. Tufvesson, A. F. Molisch, and C. F. Mecklenbräuker, "The (in-) validity of the WSSUS assumption in vehicular radio channels." in *PIMRC*, 2012, pp. 1757–1762.

[4] G. Matz, "On non-WSSUS wireless fading channels," *IEEE Transactions on Wireless Communications*, vol. 4, no. 5, pp. 2465–2478, 2005.

[5] L. Bernado, T. Zemen, F. Tufvesson, A. F. Molisch, and C. F. Mecklenbräuker, "Delay and doppler spreads of nonstationary vehicular channels for safety-relevant scenarios," *IEEE Transactions on Vehicular Technology*, vol. 63, no. 1, pp. 82–93, 2014.

[6] R. He, A. F. Molisch, F. Tufvesson, Z. Zhong, B. Ai, and T. Zhang, "Vehicle-to-vehicle propagation models with large vehicle obstructions," *IEEE Transactions on Intelligent Transportation Systems*, vol. 15, no. 5, pp. 2237–2248, 2014.

[7] Y. Shui, F. Li, J. Yu, W. Chen, C. Li, K. Yang, and F. Chang, "Vehicle-to-vehicle radio channel characteristics for congestion scenario in dense urban region at 5.9 GHz," *International Journal of Antennas and Propagation*, vol. 2018, 2018.

[8] J. Kunisch and J. Pamp, "Wideband car-to-car radio channel measurements and model at 5.9 GHz," in *Vehicular Technology Conference, 2008. VTC 2008-Fall. IEEE 68th*. IEEE, 2008, pp. 1–5.

[9] "Technical specification group radio access network; vehicle-to-everything (V2X) services based on LTE; user equipment (UE) radio transmission and reception. TR 36.786 v14.0.0," 3GPP, Tech. Rep., 2017.

[10] P. Laly, D. P. Gaillot, M. Liénard, P. Degauque, E. Tanghe, W. Joseph, and L. Martens, "Flexible real-time MIMO channel sounder for multi-dimensional polarimetric parameter estimation," in *IEEE Conference on Antenna Measurements & Applications (CAMA)*. IEEE, 2015, pp. 1–3.

[11] E. S. Sousa, V. M. Jovanovic, and C. Daigneault, "Delay spread measurements for the digital cellular channel in Toronto," *IEEE Transactions on Vehicular Technology*, vol. 43, no. 4, pp. 837–847, 1994.

[12] A. Algans, K. I. Pedersen, and P. E. Mogensen, "Experimental analysis of the joint statistical properties of azimuth spread, delay spread, and shadow fading," *IEEE Journal on selected areas in communications*, vol. 20, no. 3, pp. 523–531, 2002.

[13] V. M. Rodrigo-Peñarrocha, J. Reig, L. Rubio, H. Fernández, and S. Loredo, "Analysis of small-scale fading distributions in vehicle-to-vehicle communications," *Mobile Information Systems*, vol. 2016, 2016.

[14] D. W. Matolak and J. Frolik, "Worse-than-Rayleigh fading: Experimental results and theoretical models," *IEEE Communications Magazine*, vol. 49, no. 4, 2011.

[15] J. Cheng and N. C. Beaulieu, "Maximum-likelihood based estimation of the Nakagami m parameter," *IEEE Communications letters*, vol. 5, no. 3, pp. 101–103, 2001.

[16] L. J. Greenstein, D. G. Michelson, and V. Erceg, "Moment-method estimation of the ricean k-factor," *IEEE Communications Letters*, vol. 3, no. 6, pp. 175–176, 1999.